ACS APPLIED MATERIALS & INTERFACES

Research Article

www.acsami.org

Suppression of Phase Transition in $LiTb_{0.01}Mn_{1.99}O_4$ Cathodes with Fast Li^+ Diffusion

Dong Kyu Lee,[†] Su Chul Han,[†] Docheon Ahn,[‡] Satendra Pal Singh,[†] Kee-Sun Sohn,*[,†] and Myoungho Pyo*[,†]

[†]Department of Printed Electronics Engineering in the WCU Program, Sunchon National University, Sunchon, Chonnam 540-742, Korea

[‡]Pohang Accelerator Laboratory, Pohang 790-784, Republic of Korea

Supporting Information

ABSTRACT: The structural characteristics of terbium-doped spinel $LiTb_xMn_{2-x}O_4$ related to the electrochemical performance were studied as the cathode in lithium-ion batteries. We chose terbium as the dopant, which is a well-known mixed-valent cation (3+/4+), expecting that it would provide structural stabilization and improve the power density. $LiTb_xMn_{2-x}O_4$ revealed that terbium doping significantly affected the lattice structure and lithium-ion diffusion during charge−discharge cycles, resulting in an enhanced capacity retention and rate capability at an extremely small amount of terbium doping ($LiTb_{0.01}Mn_{1.99}O_4$). The absence of two-cubic phase formation in the delithiated state and a tetragonal phase in the overlithiated state, along with a reduced dimensional change of the main cubic phase during charge−discharge, provided $LiTb_{0.01}Mn_{1.99}O_4$ with structural stability at both room temperature and 60 °C. The fast lithium-ion diffusion resulted in reduced polarization, which became more conspicuous as the *C* rates increased. As a result, the power density of $LiTb_{0.01}Mn_{1.99}O_4$, which was similar to that of $LiMn_2O_4$ at 1*C* (476.1 $W{\cdot}kg^{-1}$ for $LiMn_2O_4$ vs 487.0 $W{\cdot}kg^{-1}$ for $LiTb_{0.01}Mn_{1.99}O_4$), was greatly improved at higher *C* rates. For example, the power density of $LiTb_{0.01}Mn_{1.99}O_4$ was improved to 4000 and 6000 $W{\cdot}kg^{-1}$ at 10 and 20, respectively, compared with 3120 and 3320 $W{\cdot}kg^{-1}$ for pristine $LiMn_2O_4$.

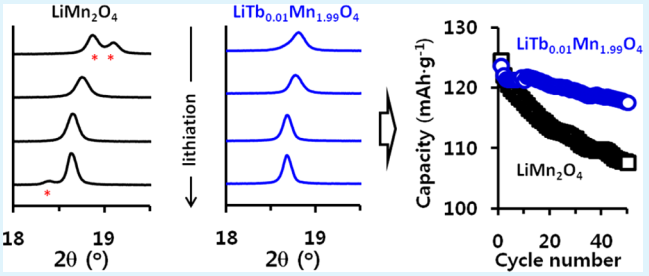

KEYWORDS: *$LiMn_2O_4$, cathode, doping, terbium, lithium-ion batteries*

1. INTRODUCTION

During the past 2 decades, the structural modification of spinel $LiMn_2O_4$ (LMO) has been extensively studied to realize the implementation of LMO-based lithium-ion batteries (LIBs) in electric vehicles by improving the capacity retention particularly at high temperatures (50−60 °C) and/or maximizing the power density.[1] These research efforts have included fine control of the LMO particle morphology, such as nanoscale regulation of the particle sizes[2−4] or inactivation of the particle surfaces by coating.[5−9] Although some of these developments have proven effective in the enhancement of the cyclability and in the rate capability, the commercial production of LMO via these methods seems to be problematic because of the complexity of the production process and increases in production costs. In this regard, tailoring the lattice structure by substituting other metal ions for manganese has been actively investigated because doping is the most adaptable to commercial production.[10−15]

The doping of electroinactive species is based mainly on the idea that the incorporation of dopants increases the average valence state of manganese,[16−20] suppressing structural distortion via the Jahn−Teller effect.[21] Doping can also modify the lattice dimension and/or slightly change the atomic arrangement in a unit cell, which confers structural integrity to LMO. The doping of electroinactive species, however, inevitably decreases the capacity attainable from a $Mn^{3+/4+}$ redox process. Moreover, the substitution of Mn^{3+} by elements heavier than the atomic weight of manganese further decreases the specific capacity of doped LMO. Lanthanide doping can also fall into this category.[22−29] Most previous reports on lanthanide doping to LMO, however, have shown that doped LMO exhibits the best performance at a small lanthanide content (less than 2.0 mol % with respect to manganese), suggesting that the negative effect on a gravimetric capacity, which is caused by heavy-atom doping, could be negligible. In addition, because some lanthanides can exist at mixed valences of 3+ and 4+ in oxides, the decrease in the theoretical capacity that is due to a reduction in the Mn^{3+} content can be further alleviated.

In this work, we revisited doping studies for improving the electrochemical performance of LMO. We address the effect of terbium, which is a well-known mixed-valent lanthanide (3+/

Received: September 15, 2012
Accepted: November 18, 2012
Published: November 19, 2012

   dx.doi.org/10.1021/am302003r | ACS Appl. Mater. Interfaces 2012, 4, 6842−6848

4+), incorporated to LMO. Impurity-free $LiTb_{0.01}Mn_{1.99}O_4$ shows that a resistance to phase transition (structural integrity) contributes to a significant improvement in the cyclability. Terbium doping also facilitates lithium-ion diffusion, resulting in a greater capacity and a higher discharge potential (thus, higher power density) than pristine LMO with increasing C rates. It is noteworthy that, to the best of our knowledge, there have been a few reports on the suppression of phase transitions at both ends (the absence of two-cubic phase formation in the delithiated state and a tetragonal phase in the overlithiated state) for LMO doped with light atoms at high contents.[22,23] However, no results showing similar behaviors for lanthanide-doped LMO at a substantially low dopant level were reported. Moreover, in most previous reports on lanthanide-doped LMO, lanthanides were utilized as codopants and, thus, it was difficult to clarify the effect of lanthanide.[24−27] The use of lanthanide as a single dopant in LMO has been examined in a limited number of papers.[28−31] There have been no reports on the effects of terbium doping on the structural and electrochemical characteristics of LMO.

2. EXPERIMENTAL SECTION

Except for the use of $Tb(CH_3COO)_3{\cdot}xH_2O$, the synthetic procedure of $LiTb_xMn_{2-x}O_4$ (x = 0, 0.01, 0.02, 0.04) via a citric acid assisted sol−gel method was similar to that in our previous report.[12]

Conventional powder X-ray diffraction (XRD) patterns were recorded for characterization of synthesized $LiTb_xMn_{2-x}O_4$ (Rigaku ULTIMA 4). The synchrotron-radiation powder XRD patterns were collected at beamline 9B at the Pohang Accelerator Laboratory (PLS II), Korea. Data were collected at room temperature (RT) from 15 to 135° (0.01° step) with an incident wavelength of 1.54750 Å. The particle size and morphology were characterized with a Hitachi S3500 field-emission scanning electron microscope. High-resolution transmission electron microscope investigations were performed on a JEOL 2100 instrument with an accelerating voltage of 200 kV. The specimens were prepared by the grinding and dispersion of a powder in ethanol by an ultrasonic treatment for 5 min. The suspensions were dropped on standard holey carbon/copper grids. Measurements of the lattice fringe spacing recorded in high-resolution transmission electron microscopy (HRTEM) micrographs were made with digital image analysis of the reciprocal space parameters. X-ray photoelectron spectroscopy (XPS) was carried out with a Thermo Fisher (K-Alpha) electron spectrometer with an Al Kα X-ray source (excitation energy = 1486.6 eV). The energy scale was adjusted with respect to the carbon peak (C 1s) spectra at 284.5 eV. To evaluate the amount of manganese dissolved in the electrolyte, synthesized powders were soaked in electrolytes at 60 °C for 7 days. After filtration, the manganese concentrations of the electrolytes were determined by inductively coupled plasma atomic emission spectroscopy (ICP-AES; Perkin Elmer 3000DC).

The fabrication of 2032 coin cells for electrochemical measurements has been described elsewhere.[12] A galvanostatic charge−discharge (C−D) cycle test was performed with an automatic WBCS 3000 battery cycler (WonATech) in a potential range of 3.0−4.5 V vs Li/Li^+. The diffusion coefficient of lithium ions was determined with the galvanostatic intermittent titration technique (GITT). The fully charged cells were discharged sequentially at 0.05C for 30 min and allowed to relax to an open-circuit potential for 2 h. Electrochemical impedance spectroscopy (EIS) was carried out by applying a 10 mV alternating-current signal over a frequency range of 10^{-1}−10^5 Hz (PARSTAT 2273).

3. RESULTS AND DISCUSSION

Morphological studies of as-synthesized $LiTb_xMn_{2-x}O_4$ (x = 0, 0.01, 0.02, 0.04) powders, examined by field-emission scanning electron microscopy (FESEM), showed no distinctive difference with terbium contents (see Figure S1 in the Supporting Information). The size of most particles ranged from 150 to 200 nm, indicating that the incorporation of terbium does not affect the crystal growth mechanism of the LMO spinel. The HRTEM image of $LiTb_{0.01}Mn_{1.99}O_4$, shown in Figure S2 in the Supporting Information, also demonstrates a well-crystallized hexagonal packing pattern with (002), (220), and (111) lattice fringes of interplanar spacing of ca. 0.39, 0.28, and 0.45 nm, respectively. The selected-area electron diffraction (SAED) pattern taken at the [110] zone axis indicated that all diffraction spots could be indexed with the $Fd\bar{3}m$ space group.

Phase-Pure $LiTb_xMn_{2-x}O_4$ with a Reduced Cell Dimension. The synchrotron-radiation XRD patterns of as-synthesized $LiTb_xMn_{2-x}O_4$ are shown in Figure 1. All of the patterns could be indexed in the $Fd\bar{3}m$ space group, indicating again that terbium doping does not affect the formation of a cubic spinel. An impurity, identified as $TbMn_2O_5$ (ICSD no. 500294, orthorhombic $Pbam$, a = 7.3420 Å, b = 8.5270 Å, and c = 5.6467 Å), was also present. $LiTb_{0.01}Mn_{1.99}O_4$ showed negligible amounts of impurities (Figure 1B), which were not identifiable with a conventional X-ray diffractometer, indicating that most terbium atoms were incorporated into a spinel lattice at this composition. However, the diffraction peaks resulting from the impurity (2θ = 29.02 and 31.01°) became evident as the terbium content was increased further. Significant amounts

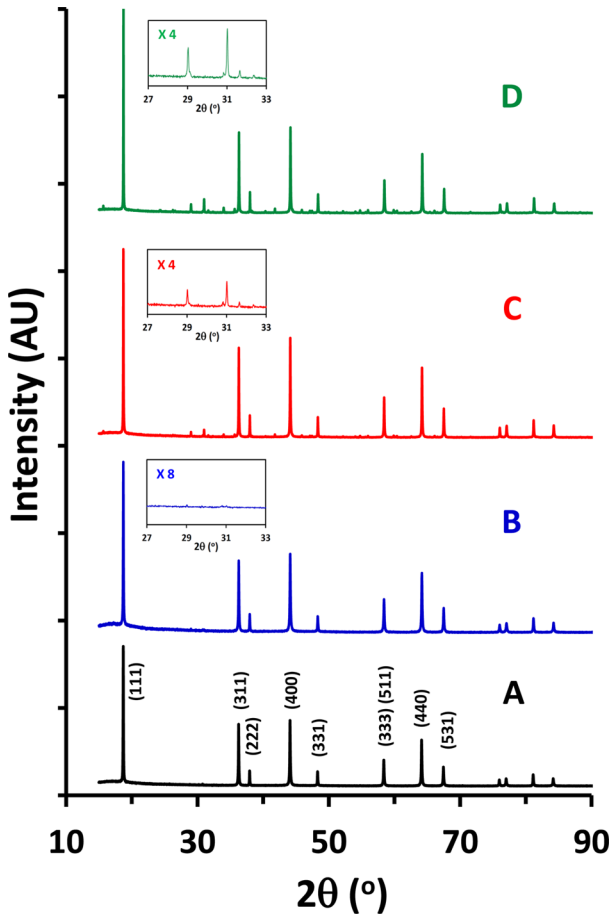

Figure 1. Synchrotron-radiation XRD patterns of (A) LMO, (B) $LiTb_{0.01}Mn_{1.99}O_4$, (C) $LiTb_{0.02}Mn_{1.98}O_4$, and (D) $LiTb_{0.04}Mn_{1.96}O_4$. The insets are magnified XRD patterns for a comparison of the $TbMn_2O_5$ impurity peaks.

dx.doi.org/10.1021/am302003r | ACS Appl. Mater. Interfaces 2012, 4, 6842−6848

of impurities were detectable for x = 0.02 and 0.04 in $LiTb_xMn_{2-x}O_4$ (insets of Figure 1C,D). The relative peak height at 31.01° shown in Figure 1D was 1.9 times higher than that shown in Figure 1C. Assuming that the intensity due to impurity was directly dependent on the mole fraction of $TbMn_2O_5$ in a powder sample, this ratio can be considered an indication that the sample of Figure 1D contains 1.9 times as much $TbMn_2O_5$ as that of Figure 1C. Note that this value should be close to 3.0 if all terbium added more than the amount necessary for the formation of phase-pure $LiTb_{0.01}Mn_{1.99}O_4$ to produce the impurity $TbMn_2O_5$. Therefore, we inferred that the amounts of terbium incorporated into a spinel lattice would continuously increase along with increases in the total amount of terbium, albeit substantial amounts of impurities were detected in $LiTb_{0.02}Mn_{1.98}O_4$ and $LiTb_{0.04}Mn_{1.96}O_4$. It is worth mentioning that XPS studies revealed terbium/manganese ratios of 0.008/0.992 and 0.015/0.985 (similar to 0.02/1.98 and 0.04/1.96) for $LiTb_{0.02}Mn_{1.98}O_4$ and $LiTb_{0.04}Mn_{1.96}O_4$, respectively, which excluded the possibility of surface-localized $TbMn_2O_5$.

The cell parameter changes with terbium doping, determined by Le Bail fitting, indicated that terbium doping strongly affects the cell dimensions. The unit cell contracted gradually from 8.239 Å (LMO) to 8.231 ($LiTb_{0.01}Mn_{1.99}O_4$), 8.227 ($LiTb_{0.02}Mn_{1.98}O_4$), and 8.218 Å ($LiTb_{0.04}Mn_{1.96}O_4$) with an increase in the terbium content. Because the ionic radius of Tb^{3+} in VI coordination (0.923 Å) is larger than that of Mn^{3+} (0.645 Å for high spin), the decrease in the cell dimensions with doping was interesting but not surprising. Similar behaviors have previously been reported,[15,16,30,32] indicating that the ionic radius of a dopant was not directly reflected by the change in the unit cell dimensions.

$LiTb_{0.01}Mn_{1.99}O_4$ with an Enhanced Energy Density. Discharge profiles of $LiTb_xMn_{2-x}O_4$ exhibited remarkable changes in both the specific capacity and plateau potential with terbium doping. Figure 2 shows the second discharge

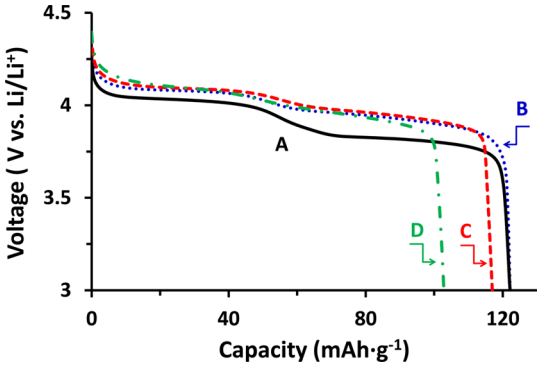

Figure 2. Discharge profiles of (A) LMO, (B) $LiTb_{0.01}Mn_{1.99}O_4$, (C) $LiTb_{0.02}Mn_{1.98}O_4$, and (D) $LiTb_{0.04}Mn_{1.96}O_4$ at 1*C*.

curves of (A) LMO, (B) $LiTb_{0.01}Mn_{1.99}O_4$, (C) $LiTb_{0.02}Mn_{1.98}O_4$, and (D) $LiTb_{0.04}Mn_{1.96}O_4$ at 1*C*. $LiTb_{0.01}Mn_{1.99}O_4$ represented a similar specific capacity to LMO (122.1 mA·h·g^{-1}) because of the small dopant concentration and the mixed valence of terbium. Further terbium doping, however, induced a gradual decrease in the specific capacities (117.0 mA·h·g^{-1} for $LiTb_{0.02}Mn_{1.98}O_4$ and 102.8 mA·h·g^{-1} for $LiTb_{0.04}Mn_{1.96}O_4$). The decrease in the specific capacities of $LiTb_{0.02}Mn_{1.98}O_4$ and $LiTb_{0.04}Mn_{1.96}O_4$ can be related to the presence of an electrochemically inactive $TbMn_2O_5$ impurity, but the extent of the capacity reduction was somewhat larger than expected. This is because $TbMn_2O_5$ not only decreases the amount of active material ($LiTb_xMn_{2-x}O_4$) but also disturbs the local electric field. $TbMn_2O_5$ is a well-known ferroelectric material[33] that can perturb the electromagnetic environment of $LiTb_xMn_{2-x}O_4$ in the vicinity of $TbMn_2O_5$ microcrystalline domains. Note that impurity-free $LiTb_{0.01}Mn_{1.99}O_4$ without the ferroelectric disturbance showed a specific capacity identical with that of pristine LMO. (Considering $LiTb_{0.01}(Mn^{3+})_{0.995}(Mn^{4+})_{0.995}O_4$, the theoretical capacity of $LiTb_{0.01}Mn_{1.99}O_4$ is 146.4 mA·h·g^{-1}, which is similar to 148.2 mA·h·g^{-1} of LMO.)

Another interesting feature of terbium doping is the mitigation of polarization. Discharge plateaus of $LiTb_xMn_{2-x}O_4$ were maintained at the same voltage, which was higher than that of LMO, regardless of the extent of terbium doping. This indicates that the existence of an impurity does not affect the electrochemical kinetics of electroactive (i.e., unaffected by the ferroelectric disturbance) $LiTb_xMn_{2-x}O_4$. Mitigation of the overpotential by as much as 120 mV in $LiTb_xMn_{2-x}O_4$ resulted in a greater energy density of $LiTb_{0.01}Mn_{1.99}O_4$ (120 mW·h·g^{-1}) and $LiTb_{0.02}Mn_{1.98}O_4$ (118.7 mW·h·g^{-1}) compared with LMO (109.8 mW·h·g^{-1}).

In order to confirm the cause of reduced polarization in $LiTb_xMn_{2-x}O_4$, the *C*-rate dependences for (A) LMO and (B) $LiTb_{0.01}Mn_{1.99}O_4$ were compared. Figure 3 (top panel) shows

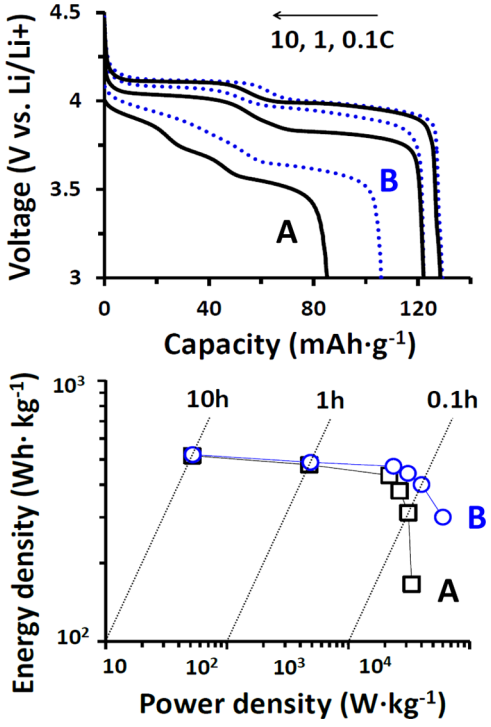

Figure 3. (top) Discharge profiles and (bottom) Ragone plots of (A) LMO and (B) $LiTb_{0.01}Mn_{1.99}O_4$ at various *C* rates.

the discharge curves scanned at 0.1, 1, and 10*C*. It is evident that the differences in the plateau potentials at 0.1*C* were negligible, suggesting that the effect of terbium doping on the overpotential reduction (due to charge transfer and/or solid-state lithium-ion diffusion) was not distinct at a slow scan. The increase of the *C* rates to 1 and 10*C*, on the other hand, revealed that the differences in both the specific capacity and the plateau potential with increasing *C* rates became

dx.doi.org/10.1021/am302003r | ACS Appl. Mater. Interfaces 2012, 4, 6842−6848

conspicuous between LMO and $LiTb_{0.01}Mn_{1.99}O_4$. To demonstrate the usefulness of $LiTb_{0.01}Mn_{1.99}O_4$, at high *C* rates in particular, we compared the energy and power densities for LMO and $LiTb_{0.01}Mn_{1.99}O_4$ with a Ragone plot (Figure 3, bottom panel). The energy density was calculated on the basis of the weight of the active cathode material by integrating the area under the discharge curves, and the power density was obtained by dividing the energy density by the discharge time. The Ragone plot clearly indicated that $LiTb_{0.01}Mn_{1.99}O_4$ delivered significantly higher energy and power densities than LMO at high *C* rates. For example, $LiTb_{0.01}Mn_{1.99}O_4$ showed an energy density of 300 $W{\cdot}h{\cdot}kg^{-1}$ and a power density of 6000 $W{\cdot}kg^{-1}$ at 20*C*, in contrast with 166 $W{\cdot}h{\cdot}kg^{-1}$ and 3320 $W{\cdot}kg^{-1}$ for LMO, respectively, indicating that terbium-doped LMO could be a promising candidate for the development of high-rate cathode materials.

Because the logarithmic decrease in the capacity with the *C*-rate increase is a typical behavior when an electrochemical process is governed by lithium-ion diffusion,[34] Figure 3 implies that, although both materials are in a regime of controlled solid-state lithium-ion diffusion, lithium transport facilitated by terbium doping in $LiTb_{0.01}Mn_{1.99}O_4$ diminished a capacity reduction and a plateau potential at high *C* rates. To further confirm this point, the lithium-ion diffusivity was evaluated by the GITT. Figure 4 shows the evolution of diffusion coefficients

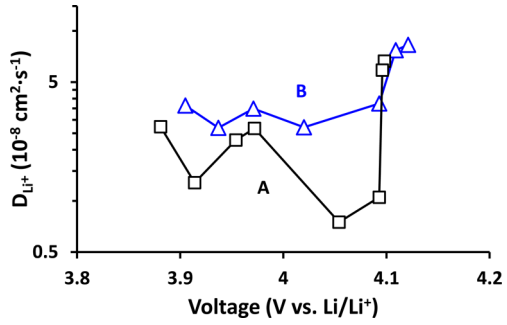

Figure 4. Evolution of diffusion coefficients of (A) LMO and (B) $LiTb_{0.01}Mn_{1.99}O_4$, calculated by the GITT.

for (A) LMO and (B) $LiTb_{0.01}Mn_{1.99}O_4$. The diffusion coefficient changes in LMO with the potential exhibited a W shape within a range of 6.5×10^{-9}–6.6×10^{-8} $cm^2{\cdot}s^{-1}$, which was in good agreement with previous reports.[35] In contrast, $LiTb_{0.01}Mn_{1.99}O_4$ exhibited rather smooth changes with the lowest diffusion coefficient of 2.6×10^{-8} $cm^2{\cdot}s^{-1}$. In particular, the absence of a deep valley at 4.05 V is interesting because two cubic phases were expected to begin to form at this potential.

$LiTb_{0.01}Mn_{1.99}O_4$ with a High Capacity Retention. The effect of terbium doping on the capacity retention was also examined. Figure 5 compares the discharge capacity fading during 50 cycles at 1C. The improvement of the capacity fading by terbium doping was evident both at RT and at 60 °C. The capacity behavior at RT shows that terbium doping for $x = 0.02$ and 0.04 decreases the initial capacity because of $TbMn_2O_5$ impurities, as explained in section 3.1. The fading for all three samples, however, was greatly alleviated. An 86.4% retention of the initial capacity after 50 cycles for LMO was enhanced to ca. 95% for all three samples (95.1% for $x = 0.01$, 94.6% for $x = 0.02$, and 94.8% for $x = 0.01$ in $LiTb_xMn_{2-x}O_4$). The contribution of terbium doping can be further confirmed at 60 °C (Figure 5, bottom panel). In contrast with 62.0%

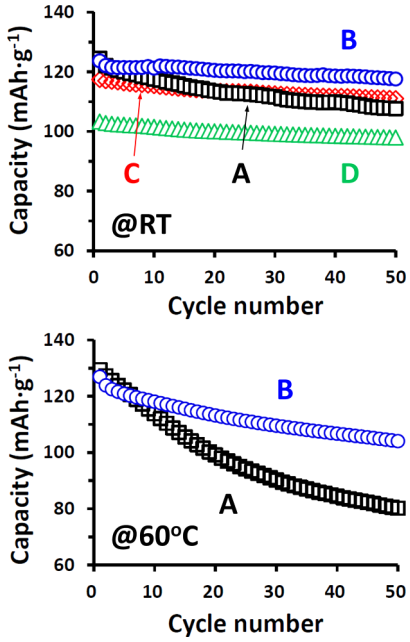

Figure 5. Capacity retention of (A) LMO, (B) $LiTb_{0.01}Mn_{1.99}O_4$, (C) $LiTb_{0.02}Mn_{1.98}O_4$, and (D) $LiTb_{0.04}Mn_{1.96}O_4$ at 1*C*: (top) RT; (bottom) 60 °C.

capacity retention for LMO, $LiTb_{0.01}Mn_{1.99}O_4$ retained 81.9% of its initial capacity after 50 cycles.

The changes in the EIS spectra after 2 and 50 C−D cycles at 60 °C were compared between (A) pristine LMO and (B) $LiTb_{0.01}Mn_{1.99}O_4$. The Nyquist plots are shown in Figure 6. To

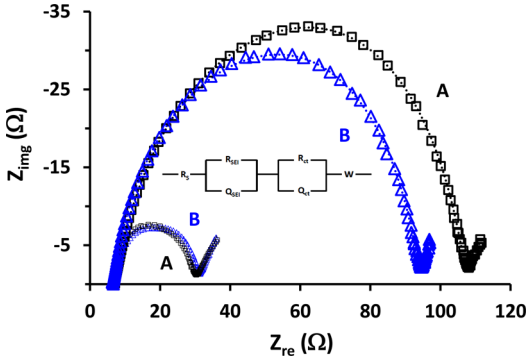

Figure 6. EIS spectra of (A) LMO and (B) $LiTb_{0.01}Mn_{1.99}O_4$ after 2 and 50 C−D cycles. Dotted lines indicate fitting results, which are based on the equivalent circuit shown in the inset. R_s = serial resistance; R_{SEI} and Q_{SEI} = resistance and constant phase element for a solid electrolyte interface; R_{ct} and Q_{ct} = resistance and constant phase element for charge transfer; *W* = Warburg impedance.

extract parameter values, the spectra were fitted with *ZView* software with an equivalent circuit shown in the inset of Figure 6 (for the parameter symbols, refer to the figure caption). All curve fittings were well-matched with the Nyquist plot with an acceptable χ^2 of less than 0.0005. After 2 C−D cycles, R_{SEI} and R_{ct} were 10.2 and 13.0 Ω for LMO and 13.7 and 9.9 Ω for $LiTb_{0.01}Mn_{1.99}O_4$, respectively, revealing a negligible difference. After 50 C−D cycles, the resistances significantly increased for both samples, resulting in R_{SEI} = 39.3 Ω and R_{ct} = 60.3 Ω for LMO and R_{SEI} = 43.6 Ω and R_{ct} = 43.5 Ω for $LiTb_{0.01}Mn_{1.99}O_4$. This indicated that the improved capacity retention for

dx.doi.org/10.1021/am302003r | ACS Appl. Mater. Interfaces 2012, 4, 6842−6848

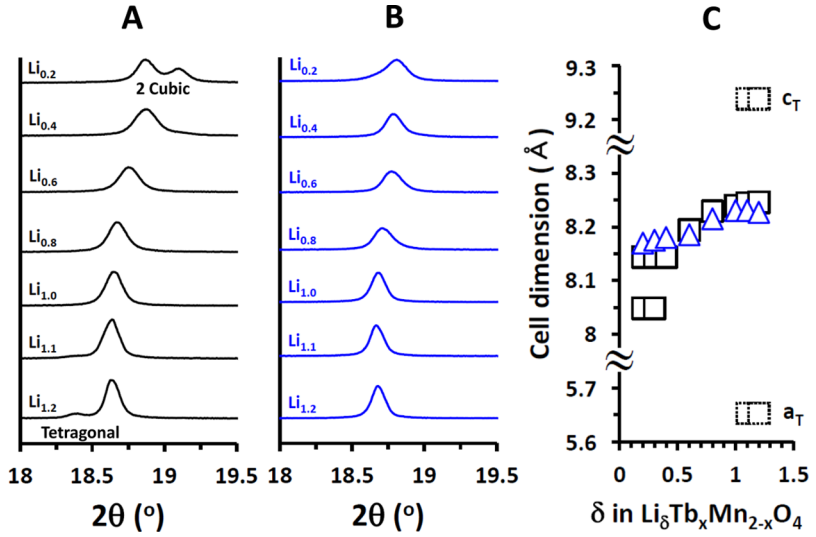

Figure 7. Evolution of the (111) diffraction peaks of (A) LMO and (B) $LiTb_{0.01}Mn_{1.99}O_4$ with changes in the depths of discharge. Part C shows cell parameter changes corresponding to XRD patterns: (squares) LMO; (triangles) $LiTb_{0.01}Mn_{1.99}O_4$. a_T and c_T denote the *a*- and *c*-axis unit cell dimensions of a tetragonal phase in LMO.

Table 1. Summary of Structural Refinement of LMO and $LiTb_{0.01}Mn_{1.99}O_4$ by a Rietveld Method Using a Cubic $Fd\bar{3}m$ Space Group

	LMO (a = 8.23936(1) Å, R_p = 7.45, R_{wp} = 9.56, R_e = 8.54, χ^2 = 1.26)					$LiTb_{0.01}Mn_{1.99}O_4$ (a = 8.23315(1) Å, R_p = 6.47, R_{wp} = 7.92, R_e = 6.17, χ^2 = 1.64)				
atomic position	x	y	z	occupancy	thermal factor	x	y	z	occupancy	thermal factor
$[Li]_{8a}$	0.1250	0.1250	0.1250	0.04167	0.2(2)	0.1250	0.1250	0.1250	0.04167	0.2(2)
$[Mn]_{16d}$	0.5000	0.5000	0.5000	0.08333	0.22(2)	0.5000	0.5000	0.5000	0.08292	0.033(2)
$[Tb]_{16d}$						0.5000	0.5000	0.5000	0.00042	0.033(2)
$[O]_{32e}$	0.2620(3)	0.2620(1)	0.2620(1)	0.16667	0.61(4)	0.26107(9)	0.2611(1)	0.26107(9)	0.16667	0.41(3)
		Li–O			Mn (Tb)–O		Li–O		Mn (Tb)–O	
distance (Å)		1.955(1)			1.966(1)		1.9404(8)		1.9714(8)	

$LiTb_{0.01}Mn_{1.99}O_4$ could be attributed to the smaller increase in R_{ct} compared with LMO.

Suppressed Phase Transition in $LiTb_{0.01}Mn_{1.99}O_4$. In general, an increase in R_{ct} and, thus, capacity fading in LMO can be affected by various factors: (1) oxygen deficiency;[36,37] (2) manganese dissolution into the electrolyte;[38−40] (3) a lattice mismatch, resulting from the coexistence of cubic and tetragonal phases on the surface of LMO ($Li_2Mn_2O_4$) and related Jahn−Teller distortion;[23] (4) the formation of two cubic phases and thus the development of a microstrain.[41] Among them, oxygen loss was not expected to occur because $LiTb_{0.01}Mn_{1.99}O_4$ was within a range of lithium contents greater than 0.15 during cycling.[36] In addition, LMO and $LiTb_{0.01}Mn_{1.99}O_4$ showed no typical shoulder occurring at 3.2 V during discharge,[37] indicating that the oxygen deficiency in both samples was not a factor in this work. Manganese dissolution has been known to account for some fraction of the total capacity fading.[39,40] However, we found no changes in the manganese concentration of the electrolyte with terbium doping, for which LMO and $LiTb_xMn_{2-x}O_4$ (x = 0.01, 0.02, and 0.04) powders were soaked in the electrolyte for 7 days and the manganese concentration was confirmed by ICP-AES.

To correlate an improvement in the capacity retention with the lattice stability, we compared the evolution of the XRD patterns at various depths of discharge. Parts A and B of Figure 7 clearly reveal that, while (111) diffraction of LMO in a delithiated state ($Li_{0.2}$; i.e., δ = 0.2 in $Li_\delta Mn_2O_4$ or $Li_\delta Tb_{0.01}Mn_{1.99}O_4$; the same notation will be used hereafter) splits into two cubic phases (2θ = 18.870 and 19.095°),[42] $LiTb_{0.01}Mn_{1.99}O_4$ maintained one cubic phase (2θ = 18.810°). The subsequent discharge continuously shifted the 2θ peak position toward a lower diffraction angle. For $Li_{1.0}$, the $Fd\bar{3}m$ cubic cell dimensions were 8.239 Å (2θ = 18.650°) and 8.231 Å (2θ = 18.670°) for LMO and $LiTb_{0.01}Mn_{1.99}O_4$, respectively. Further discharge revealed the formation of a tetragonal phase in LMO, as expected,[43,44] but quite interestingly, no phase transformation was observed in $LiTb_{0.01}Mn_{1.99}O_4$. Moreover, the cubic (111) peak position stayed at ca. 18.670° during overlithiation from $Li_{1.0}$ to $Li_{1.2}$, in contrast with a discernible peak shift from 18.650 to 18.635°.

Figure 7C summarizes the changes in the cell parameters of LMO and $LiTb_{0.01}Mn_{1.99}O_4$ with the depths of discharge. The results indicate that, besides suppression of the formation of two cubic phases in a delithiated state and a tetragonal phase in an overlithiated state, the dimensional change in the major cubic phase with discharge was also alleviated in $LiTb_{0.01}Mn_{1.99}O_4$. This result implies that the excellent cyclability of $LiTb_{0.01}Mn_{1.99}O_4$ resulted from structural integrity (resistance to the structural variation). It should be mentioned that no previous reports have addressed similar results (i.e., the suppression of phase transition at both ends and simultaneous mitigation of dimensional change in the major cubic phase) for a dopant content as small as that of $LiTb_{0.01}Mn_{1.99}O_4$.

Interatomic Distance Changes in $LiTb_{0.01}Mn_{1.99}O_4$. For a better understanding of the effect of terbium doping on the cell parameters and atomic arrangements, Rietveld refinement was performed with the *FULLPROF* package.[45] In the refinements, a pseudo-Voigt function and a linear interpolation between the set background points with refinable heights were used to define the profile shape and ackground, respectively. With the exception of the occupancy parameters of the ions, which were fixed at the nominal composition (x = 0.01), all other parameters such as the scale factor, zero correction, background, half-width parameters, the mixing parameters, lattice parameters, positional coordinates, and thermal parameters were varied during the course of refinement. Figure S3 in the Supporting Information depicts the Rietveld fits for pristine LMO and $LiTb_{0.01}Mn_{1.99}O_4$ with a cubic spinel in the $Fd\bar{3}m$ space group. The refined parameters are summarized in Table 1.

Very good fits between the observed and calculated data were obtained with reasonably good agreement factors. The values of the agreement factors for the pristine LMO and $LiTb_{0.01}Mn_{1.99}O_4$ were R_p = 7.45 and 6.47, R_{wp} = 9.56 and 7.92, R_e = 8.54 and 6.17, and χ^2 = 1.26 and 1.64, respectively. The refinement results indicated that the change in the unit cell dimensions by terbium doping was not proportionally reflected by a change in the interatomic distances. The Li−O distance was significantly decreased by terbium doping [1.955(1)−1.9404(8) Å], but the Mn−O distance was expanded slightly [1.966(1)−1.9714(8) Å]. Because Li^+-ion diffusion occurs through empty tetrahedra and octahedra interconnected with one another by common faces and edges, it is believed that the concerted contraction of a LiO_4 tetrahedron and the expansion of neighboring MnO_6 octahedra are mainly responsible to the fast electrochemical kinetics.[46] The enhanced structural integrity of $LiTb_{0.01}Mn_{1.99}O_4$, on the other hand, appears to be related to a decrease in the unit cell dimensions rather than to a change in the individual interatomic distances.

4. CONCLUSIONS

Impurity-free terbium-doped spinel $LiTb_{0.01}Mn_{1.99}O_4$, synthesized via a sol−gel method, showed excellent rate capability with a greater capacity and less overpotential, relative to undoped LMO, which resulted in an improved power density. The spinel structure was also stabilized by terbium doping (i.e., resistance against structural deformation). The capacity fading was greatly alleviated at both RT and 60 °C, which was ascribed to the suppression of phase transition to two-cubic phases in the delithiated state and to a tetragonal phase in the overlithiated state. It was disclosed that, while the concerted contraction of a LiO_4 tetrahedron and the expansion of neighboring MnO_6 octahedra contributed to fast electrochemical kinetics, a decrease in the unit cell dimensions resulted in the enhanced structural integrity of $LiTb_{0.01}Mn_{1.99}O_4$.

■ ASSOCIATED CONTENT

Supporting Information

FESEM images of $LiTb_xMn_{2-x}O_4$ spinels with various terbium contents (Figure S1), HRTEM image and SAED pattern of $LiTb_{0.01}Mn_{1.99}O_4$ (Figure S2), and profiles obtained after full-pattern Rietveld refinements with synchrotron powder XRD data for LMO and $LiTb_{0.01}Mn_{1.99}O_4$ (Figure S3). This material is available free of charge via the Internet at http://pubs.acs.org.

■ AUTHOR INFORMATION

Corresponding Author

*E-mail: kssohn@sunchon.ac.kr (K.-S.S.), mho@sunchon.ac.kr (M.P.). Fax: +82 61 750 5260.

Notes

The authors declare no competing financial interest.

■ ACKNOWLEDGMENTS

This research was supported by the WCU program through the Korea Science and Engineering Foundation funded by the Ministry of Education, Science and Technology (Grant R31-10022).

■ REFERENCES

(1) Fergus, J. P. *J. Power Sources* **2010**, *195*, 939−954.
(2) Arrebola, J. C.; Caballero, A.; Cruz, M.; Hernan, L.; Morales, J.; Castellon, E. R. *Adv. Funct. Mater.* **2006**, *16*, 1904−1912.
(3) Xu, H. Y.; Xie, S.; Ding, N.; Liu, B. L.; Shang, Y.; Chen, C. H. *Electrochim. Acta* **2006**, *51*, 4352−4357.
(4) Myung, S. T.; Komaba, S.; Kumagai, N.; Yashiro, H.; Chung, H. T.; Cho, T. H. *Electrochim. Acta* **2002**, *47*, 2543−2549.
(5) Sahan, H.; Goktepe, H.; Patat, S.; Ulgen, A. *Solid State Ionics* **2008**, *178*, 1837−1842.
(6) Yang, Z.; Yang, W.; Evans, D. G.; Zhao, Y.; Wei, X. *J. Power Sources* **2009**, *189*, 1147−1153.
(7) Lim, S. H.; Cho, J. *J. Electrochem. Commun.* **2008**, *10*, 1478−1481.
(8) Li, X.; Xu, Y. *J. Solid State Electrochem.* **2008**, *12*, 851−855.
(9) Liu, J.; Manthiram, A. *Chem. Mater.* **2009**, *21*, 1695−1707.
(10) Sigala, C.; Salle, A. L. G. L.; Piffard, Y.; Guyomard, D. *J. Electrochem. Soc.* **2001**, *148*, A819−A825.
(11) Shigemura, H.; Sakaebe, H.; Kageyama, H.; Kobayashi, H.; West, A. R.; Kanno, R.; Morimoto, S.; Nasu, S.; Tabuchi, M. *J. Electrochem. Soc.* **2001**, *148*, A730−A736.
(12) Prabakar, S. J. R.; Han, S. C.; Singh, S. P.; Lee, D. K.; Sohn, K.-S.; Pyo, M. *J. Power Sources* **2012**, *209*, 57−64.
(13) Ein-Eli, Y.; Howard, W. F. *J. Electrochem. Soc.* **1997**, *144*, L205−L207.
(14) Kawai, H.; Nagata, M.; Kageyama, H.; Tukamoto, H.; West, A. R. *Electrochim. Acta* **1999**, *45*, 315−327.
(15) Reddy, M. V.; Manoharan, S. S.; John, J.; Singh, B.; Rao, G. V. S.; Chowdari, B. V. R. *J. Electrochem. Soc.* **2009**, *156*, A652−A660.
(16) Guo, S.; Zhang, S.; He, X.; Pu, W.; Jiang, C.; Wan, C. *J. Electrochem. Soc.* **2008**, *155*, A760−A763.
(17) Tan, C. L.; Zhou, H. J.; Li, W. S.; Hou, X. H.; Lu, D. S.; Xu, M. Q.; Huang, Q. M. *J. Power Sources* **2008**, *184*, 408−413.
(18) Lee, Y.-S.; Kumada, N.; Yoshio, M. *J. Power Sources* **2001**, *96*, 376−384.
(19) Yi, T.; Hu, X.; Gao, K. *J. Power Sources* **2006**, *162*, 636−643.
(20) Xiao, L.; Zhao, Y.; Yang, Y.; Cao, Y.; Ai, X.; Yang, H. *Electrochim. Acta* **2008**, *54*, 545−550.
(21) Thackeray, M. M.; Shao-Horn, Y.; Kahaian, J.; Kepler, K. D.; Skinner, E.; Vaughey, J. T.; Hackney, S. A. *Electrochem. Solid-State Lett.* **1998**, *1*, 7−9.
(22) Sun, Y.-K.; Jeon, Y.-S. *J. Mater. Chem.* **1999**, *9*, 3147−3150.
(23) Park, S. H.; Park, K. S.; Sun, Y.-K.; Nahm, K. S. *J. Electrochem. Soc.* **2000**, *147*, 2116−2121.
(24) Sun, X.; Hu, X.; Shi, Y.; Li, S.; Zhou, Y. *Solid State Ionics* **2009**, *180*, 377−380.
(25) Xie, Y.; Yang, R.; Yan, L.; Qi, L.; Dai, K.; He, P. *J. Power Sources* **2007**, *168*, 272−277.
(26) Tu, J.; Zhao, X. B.; Zhuang, D. G.; Cao, G. S.; Zhu, T. J.; Tu, J. P. *Physica B* **2006**, *382*, 129−134.
(27) Arumugam, D.; Kalaignan, G. P.; Manisankar, P. *Solid State Ionics* **2008**, *179*, 580−586.
(28) Liu, H. W.; Zhang, K. L. *Mater. Lett.* **2004**, *58*, 3049−3051.
(29) Yang, S. T.; Jia, J. H.; Ding, L.; Zhang, M. C. *Electrochim. Acta* **2003**, *48*, 569−573.

(30) Singhal, R.; Das, S. R.; Tomar, M. S.; Ovideo, O.; Nieto, S.; Melgarejo, R. E.; Katiyar, R. S. *J. Power Sources* **2007**, *164*, 857−861.
(31) Sun, H.; Chen, Y.; Xu, C.; Zhu, D.; Huang, L. *J. Solid State Electrochem.* **2012**, *16*, 1247−1254.
(32) Han, S. C.; Singh, S. P.; Hwang, Y.-H.; Bae, E. G.; Park, B. K.; Sohn, K.-S.; Pyo, M. *J. Electrochem. Soc.* **2012**, *159*, A1867−A1873.
(33) Han, J.-T.; Huang, Y.-H.; Huang, W.; Goodenough, J. B. *J. Am. Chem. Soc.* **2006**, *128*, 14454−14455.
(34) Dokkoa, K.; Nakatab, N.; Kanamura, K. *J. Power Sources* **2009**, *189*, 783−785.
(35) Mohamedi, M.; Takahashi, D.; Itoh, T.; Uchida, I. *Electrochim. Acta* **2002**, *47*, 3483−3489.
(36) Chebiam, R. V.; Kannan, A. M.; Prado, F.; Manthiram, A. *Electrochem. Commun.* **2001**, *3*, 624−627.
(37) Gao, Y.; Dahn, J. R. *J. Electrochem. Soc.* **1996**, *143*, 100−114.
(38) Aoshima, T.; Okahara, K.; Kiyohara, C.; Shizuka, K. *J. Power Sources* **2001**, *97*−*98*, 377−380.
(39) Lee, J. H.; Hong, J. K.; Jang, D. H.; Sun, Y.-K.; Oh, S. M. *J. Power Sources* **2000**, *89*, 7−14.
(40) Yamane, H.; Inoue, T.; Fujita, M.; Sano, M. *J. Power Sources* **2001**, *99*, 60−65.
(41) Shin, Y.; Manthiram, A. *Electrochem. Solid-State Lett.* **2002**, *5*, A55−A58.
(42) Shin, Y.; Manthiram, A. *Chem. Mater.* **2003**, *15*, 2954−2961.
(43) Peramunage, D.; Abraham, K. M. *J. Electrochem. Soc.* **1998**, *145*, 113−1136.
(44) Ohzuku, T.; Kitagawa, M.; Hirai, T. *J. Electrochem. Soc.* **1990**, *137*, 769−775.
(45) Rodriguez-Carvajal, J. *FULLPROF*; Laboratory Leon Brillouin (CEA-CNRS) CEA/Saclay: Gif sur Yvette Cedex, France, 2006.
(46) Winter, M.; Besenhadr, J. O.; Spahr, M. E.; Novak, P. *Adv. Mater.* **1998**, *10*, 725−763.